Article

Mechanical Properties and Binary-Medium-Based Constitutive Model for Coral-Reef Limestone Samples Subjected to Uniaxial Loading

Yongtao Zhang [1,2,3], Huiwu Luo [1,3], Peishuai Chen [1,3], Enlong Liu [4,*] and Yanbin Chen [4]

1   CCCC Second Harbour Engineering Company Ltd., Wuhan 430040, China
2   School of Civil Engineering, Tongji University, Shanghai 200092, China
3   Research and Development Center of Transport Industry of Intelligent Manufacturing Technologies of Transport Infrastructure, Wuhan 430040, China
4   State Key Laboratory of Hydraulics and Mountain River Engineering, College of Water Resources and Hydropower, Sichuan University, Chengdu 610065, China
*   Correspondence: liuenlong@scu.edu.cn; Tel.: +86-028-85400398

Abstract: The mechanical and deformation mechanism of coral-reef limestone is vital for the stability and safety of infrastructures built on the ground composed of those materials. Upon loading, strain softening behavior of the coral-reef limestone occurs, usually due to the nonuniform cementation distribution, and the cementation within the samples may break up gradually and reduce the bearing capacity. In order to study their mechanical features, uniaxial compression tests were carried out in this study, and, based on the test results, a binary-medium-based constitutive model was formulated, in which, the sample was idealized, respectively, as the bonded and frictional elements. The bonded elements are composed of strong cementation and may gradually break up to transform into the frictional elements, both of which bear the external loading conjointly. In the new model, the parameters determination method was adopted based on uniaxial compression testing, and comparisons were made between the tested and computed results, which demonstrate that the model can reflect the salient features of coral-reef limestone samples, such as the strain softening and bonding breakage during the loading process. The study can provide a basis for the basic design of coral-reef limestone.

Keywords: uniaxial loading; constitutive model; breakage mechanism; binary-medium-based constitutive model

1. Introduction

With the rapid development of marine resources in the world, many geotechnical-related projects have been constructed and designed, usually encountering complex geological conditions of coral-reef limestone. The coral-reef limestone is formed from the dead bodies of corals in the geological history, which are composed of main parts of the transition zones of continents and islands. During the formation process of coral-reef limestone, combined actions, including physical sedimentation and cementations, mechanical damage, and biological reconstruction, led to the distribution of cementation actions heterogeneously within the samples. Upon loading, the cementations within the samples easily and gradually damage, which thus results in the strain softening behavior of the samples. When the coral-reef limestone is treated as foundations of infrastructures, their mechanical features have to be understood in detail, but few studies can be found on the mechanical and stress–strain descriptions of coral-reef limestone subjected to uniaxial loading conditions.

Many studies have been conducted on rock samples in terms of tests, numerical simulations, and theoretical analysis. Cargill and Shakoor [1] studied the correlations

between the compressive strength values of many kinds of rock samples in terms of the standard uniaxial compression test, the point load, the Schmidt hammer, the Los Angeles abrasion, and the slake durability tests, which demonstrate that strong linear correlations exist between the results of uniaxial compression vs. the point load and Schmidt hammer tests, the correlation for the Schmidt hammer being dependent on the rock type. Zhang et al. [2] studied the acoustic emission of three salt rocks under uniaxial compression conditions, in which the acoustic emissions (AE) properties of halite, glauberite, and gypsum during a compression stress state were studied, and it was found that the loading style and saturation condition affect the AEs of the rocks, and that the AE properties of glauberite containing an interlayer are controlled by the interlayer. Singh et al. [3] discussed an approach to predicting the creep behavior of rock salt using a uniaxial compression testing machine, in which the AE technique used in the study to explain the rock salt behavior is based on a combination of Maxwell and Hooke models, and the proposed model is able to predict the stress–strain response of rock salt with a fair accuracy in both loading and unloading conditions, as well as calculating both elastic and viscous parameters. Azarafza et al. [4,5] investigated the geotechnical and geo-engineering properties of the South Pars Zone (SPZ) marls in Assalouyeh, Iran, which have shown that an increase in the carbonate content leads to a decrease in the degradation potential and an increase in the density and strength parameters, such as durability and compressive strength; later, in 2021, they presented an experimental classification for South Pars marls (SPM), southwest of Iran, using the Schmidt hammer rebound index, marl geological classes, and SPM geo-engineering characteristics, and, according to geotechnical experiments results, the Schmidt index shows three main group variations, like Pettijohn's marl classification. Yu et al. [6] performed triaxial compression tests on semi-through jointed mudstone samples at conditions of different confining pressures and inclination angles, based on which, a binary-medium constitutive model for semi-through jointed mudstone samples was proposed, and the model shows the effects of inclination angles and confining pressures on jointed mudstone deformation features and gives good predictions both qualitatively and quantitatively. Yesiloglu, Gultekin and Gokceoglu [7] developed various non-linear prediction models for unconfined compression strength and the initial elastic modulus by employing simple and non-destructive test results, in which a dataset that included 137 cases was analyzed and the non-linear multiple regression (NLMR), adaptive-neuro fuzzy inference system (ANFIS), and artificial neural networks (ANN) were utilized as non-linear prediction algorithms. Yu et al. [8] developed a multi-field coupling experimental system for broken coal to study the effects of temperature on the evolution and distribution for the particle size of loose broken coal during the uniaxial confined compression process, which indicates that the particle gradation tended to be reasonably gradual, and, for a given stress, the particle breakage rate presented a slow increasing trend initially while accelerating later under different temperatures. Besides the above studies carried out on rocks, there is some existing research on coral-reef limestones that is limited. For example, Wan et al. [9] conducted field load tests on two large-diameter drilled shafts in coral-reef limestone formations in the Male-Airport Island Cross-sea Bridge area in the Maldives, in which the results of bi-direction O-cell testing on one 3.2 m diameter and one 1.5 m diameter drilled shaft before and after grouting in coral-reef limestone formations were reported, the two test shafts had a higher bearing capacity after grouting, and both of these values met the requirements of the shaft design. Tang et al. [10] investigated the profiles for the shallow strata of coral reefs in the southwest of the Yongshu Reef, particularly in the hydrodynamic marine environment, and established a geological model for numerical simulation, in which the simulation results showed that the coral reef stability depends on wave loads and earthquake strength and on the physical properties of coral reefs. Li et al. [11] studied the shear behavior of the coral reef limestone–concrete interface by performing direct shear tests, in which five types of interfaces—planar, sloped, arc shaped, stepped, and triangular—were used, and the results show that the shear phenomena at

the smooth and mud-filled interfaces between the coral reef limestone and concrete were characterized by the interface slip failure mode.

Even though some studies have been conducted on coral-reef limestone samples, the understanding of their mechanical features are preliminary, and much work has to be carried out in order to grasp their mechanical and deformation characteristics in detail. For coral-reef limestone, the cementations formed within them are distributed inhomogeneously, which can be gradually locally damaged and, thus, once the bigger microcracks are formed within the sample, will fail and have strain softening behavior. For the existing constitutive model for coral-reef limestone, few of them consider the influence of the inhomogeneous distribution of cementations. In addition, the strain and stress in the sample are also nonuniform, which should be considered when formulating the new constitutive model. In this study, based on the failure mechanism of coral-reef limestone samples, a binary-medium-based constitutive model was put forward that can consider the cementing breakage within the samples and the nonuniform distribution of stress and strain within the sample, followed by the determination method of model parameters, and, finally, uniaxial compressional tests were performed to calibrate the model parameters, and the comparisons between the predicted and tested results demonstrate the ability of the model, which can be a guidance in designing foundations in coral-reef limestone.
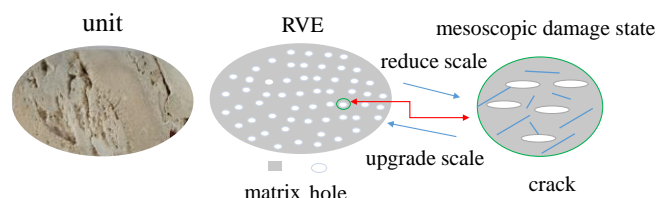
2. Constitutive Model for Coral-Reef Limestone Samples

2.1. Binary-Medium-Based Constitutive Model

2.1.1. Assumptions

The diagenesis and epigenetic evolution of coral-reef limestone are considered unique and completely different from conventional terrestrial deposition. In addition, the pore types of coral-reef limestone have shown to be complex. Thus, in order to facilitate problem analysis, uncompacted cement filling could be simplified as a problem of cementation characteristics, and uncompacted filling between diagenetic particles could be simplified as a porosity problem. The pores between cement can result in large differences in the cementation strength of coral-reef limestone, whereas pores between diagenetic particles can further exacerbate the dispersion of coral-reef limestone strength. Based on this understanding, to accurately describe the bearing characteristics of coral-reef limestone, the stress element of coral-reef limestone was decomposed with the following assumptions.

(1) At the mesoscopic scale, the material was regarded as a mixture of pores and a matrix, in which, the matrix was damaged. The macroscopic constitutive model could be established by homogenizing the mesoscopic damage state to the RVE state (representation volume element). According to the failure mechanism and microstructure analysis of coral-reef limestone, a large pore distribution and strong cementation was found between the particles. Thus, a binary medium concept [12,13] was used to establish a constitutive model, as illustrated in Figure 1.

Figure 1. Coral reef limestone—theoretical model construction schematic.

(2) According to the particle size, coral-reef limestone can be divided into four types. Analysis of the sample pore distribution characteristics showed that the larger the particle, the more uneven the pore distribution. Considering the entire formation, the particle–pore distribution could be considered uniform. Therefore, this work assumed that the particle–pores were evenly distributed. A schematic diagram of the coral-reef limestone is shown in Figure 2.

(a)

(b)

(c)

(d)

Figure 2. Coral reef limestone grain and structure type. (**a**) Block structure coral-reef limestone, (**b**) gravel structure coral-reef limestone, (**c**) gravel debris structure coral-reef limestone, and (**d**) sandy debris coral-reef limestone.

(3) The coral-reef limestone samples were basically located at the same level, and were relatively concentrated, with a small cementation difference between the coral-reef limestone samples.

2.1.2. Generalized Stress–Strain Relationship for Coral-Reef Limestone Samples

Based on the homogenization theory, the stress–strain relationship of the unit could be obtained [12,13]:

$$\sigma_{ij} = (1 - \chi)\sigma_{ij}^{b} + \chi\sigma_{ij}^{f} \tag{1}$$

$$\varepsilon_{ij} = (1 - \chi)\varepsilon_{ij}^{b} + \chi\varepsilon_{ij}^{f} \tag{2}$$

where σ_{ij} and ε_{ij} are volumetric stresses and strain of the elements, χ is the breakage rate, representing the volume rate of the frictional elements (referred to as the volume breakage rate), σ_{ij}^{b} and σ_{ij}^{f} are the stresses of the bonded elements and frictional elements, and ε_{ij}^{b} and ε_{ij}^{f} are the strain of the bonded elements and frictional elements. In addition, χ is the breakage rate, representing the volume rate of the frictional elements (referred to as the volume breakage rate), by the following expression:

$$\chi = \frac{v_f}{v} \tag{3}$$

where v_{f-} and v are the volume of the frictional elements and the elements. Because the breakage rate would vary with the strain/stress level during loading, it was deemed an internal variable with a similar meaning to the hardening parameter in plastic mechanics and damage variable in damage mechanics. Assuming the breakage rate as a function of strain:

$$\chi = f(\varepsilon_{ij}) \tag{4}$$

from Equation (1), we obtain

$$d\sigma_{ij} = (1 - \chi^{0})d\sigma_{ij}^{b} + \chi^{0}d\sigma_{ij}^{f} + d\chi(\sigma_{ij}^{f0} - \sigma_{ij}^{b0}) \tag{5}$$

where χ^{0} is the current breakage rate, and σ_{ij}^{b0} and σ_{ij}^{f0} are the current stresses of the bonded elements and frictional elements, respectively. Similarly, from Equation (2), we obtained:

$$d\varepsilon_{ij} = (1 - \chi^{0})d\varepsilon_{ij}^{b} + \chi^{0}d\varepsilon_{ij}^{f} + d\chi(\varepsilon_{ij}^{f0} - \varepsilon_{ij}^{b0}) \tag{6}$$

where ε_{ij}^{b0} and ε_{ij}^{f0} are the current strains of the bonded elements and frictional elements, respectively.

The stiffness matrices of the bonded elements and frictional elements were represented by D_{ijkl}^{b} and D_{ijkl}^{f}, respectively, and the stress–strain relationships of the bonded elements and frictional elements could be acquired by:

$$d\sigma_{ij}^{b} = D_{ijkl}^{b}d\varepsilon_{ij}^{b} \tag{7}$$

and

$$d\sigma_{ij}^{f} = D_{ijkl}^{f}d\varepsilon_{ij}^{f} \tag{8}$$

By transforming Equation (6), we obtain:

$$d\varepsilon_{ij}^{f} = \frac{1}{\chi^{0}}\left\{ d\varepsilon_{ij} - (1-\chi^{0})d\varepsilon_{ij}^{b} - d\chi(\varepsilon_{ij}^{f0} - \varepsilon_{ij}^{b0}) \right\} \tag{9}$$

By substituting Equation (9) into Equation (8), we obtain:

$$d\sigma_{ij}^{f} = \frac{D_{ijkl}^{f}}{\chi^{0}}\left\{ d\varepsilon_{kl} - (1-\chi^{0})d\varepsilon_{kl}^{b} - d\chi(\varepsilon_{kl}^{f0} - \varepsilon_{kl}^{b0}) \right\} \tag{10}$$

By substituting Equation (10) into Equation (5), we could obtain:

$$d\sigma_{ij} = (1-\chi^{0})\left\{ D_{ijkl}^{b} - D_{ijkl}^{f} \right\}d\varepsilon_{kl}^{b} + D_{ijkl}^{f}d\varepsilon_{kl} - d\chi D_{ijkl}^{f}\left\{ \varepsilon_{kl}^{f0} - \varepsilon_{kl}^{b0} \right\} \\ + d\chi\left\{ \sigma_{ij}^{f0} - \sigma_{ij}^{b0} \right\} \tag{11}$$

By introducing the local strain coefficient C_{ijkl}, we established a relationship between the strain of the bonded elements and the strain of the representative element, satisfying the following equation:

$$\varepsilon_{ij}^{b} = C_{ijkl}\varepsilon_{kl} \tag{12}$$

Thus, the incremental form is:

$$d\varepsilon_{ij}^{b} = C_{ijkl}^{0}d\varepsilon_{kl} + dC_{ijkl}\varepsilon_{kl}^{0} \tag{13}$$

where C_{ijkl} denotes the current local strain coefficient matrix.

By substituting Equation (13) into Equation (11), we have:

$$d\sigma_{ij} = \left\{ (1-\chi^{0})\left[D_{ijmn}^{b} - D_{ijmn}^{f} \right]C_{mnkl}^{0} + D_{ijkl}^{f} \right\}d\varepsilon_{kl} + \\ d\chi\left\{ \left[\sigma_{ij}^{f0} - \sigma_{ij}^{b0} \right] - D_{ijkl}^{f}\left[\varepsilon_{kl}^{f0} - \varepsilon_{kl}^{b0} \right] \right\} + (1-\chi^{0})\left\{ D_{ijmn}^{b} - D_{ijmn}^{f} \right\}dC_{mnkl}\varepsilon_{kl}^{0} \tag{14}$$

From Equations (1) and (2), we could obtain the following under the current stress–strain state:

$$\sigma_{ij}^{f0} = \left\{ \sigma_{ij}^{0} - (1-\chi^{0})\sigma_{ij}^{b0} \right\}/\chi^{0} \tag{15}$$

$$\varepsilon_{ij}^{f0} = \left\{ \varepsilon_{ij}^{0} - (1-\chi^{0})\varepsilon_{ij}^{b0} \right\}/\chi^{0} \tag{16}$$

By substituting Equations (15) and (16) into Equation (14), the expression of stress increments under the general stress state could be obtained as follows:

$$d\sigma_{ij} = \left\{ (1-\chi^{0})\left[D_{ijmn}^{b} - D_{ijmn}^{f} \right]C_{mnkl}^{0} + D_{ijkl}^{f} \right\}d\varepsilon_{kl} + (1-\chi^{0})\left\{ D_{ijmn}^{b} - D_{ijmn}^{f} \right\}\times \\ dC_{mnkl}\varepsilon_{kl}^{0} - \frac{d\chi D_{ijkl}^{f}}{\chi^{0}}\left\{ \varepsilon_{kl}^{f0} - \varepsilon_{kl}^{b0} \right\} + \frac{d\chi}{\chi^{0}}\left\{ \sigma_{ij}^{0} - \sigma_{ij}^{b0} \right\} \tag{17}$$

At the initial moment of loading, the strain would be zero, and the stress of the bonded elements would be equal to that of the frictional elements. Substituting these initial

conditions into Equation (17) gives an expression for the stress increments under the initial stress state:

$$d\sigma_{ij} = \left\{ (1 - \chi^0) \left[D^b_{ijmn} - D^f_{ijmn} \right] C^0_{mnkl} + D^f_{ijkl} \right\} d\varepsilon_{kl} \tag{18}$$

2.1.3. Stress–Strain Relationships for the Bonded Elements

The stress–strain relationship of the bonded elements is poroelastic, consisting of a solid matrix and pores. The effect of cementation reacts to the value of the elastic parameter, and is determined by the stress–strain of the initial loading section. Thus, the bonded elements are poroelastic, and the stress–strain relationship of the bonded elements is given by:

$$\left\{ \begin{array}{c} d\sigma_x \\ d\sigma_y \\ d\sigma_z \\ d\tau_{xy} \\ d\tau_{yz} \\ d\tau_{zx} \end{array} \right\}_b = \begin{bmatrix} K^b + \frac{4}{3}G^b & K^b - \frac{2}{3}G^b & K^b - \frac{2}{3}G^b & 0 & 0 & 0 \\ K^b - \frac{2}{3}G^b & K^b - \frac{2}{3}G^b & K^b - \frac{2}{3}G^b & 0 & 0 & 0 \\ K^b - \frac{2}{3}G^b & K^b - \frac{2}{3}G^b & K^b + \frac{4}{3}G^b & 0 & 0 & 0 \\ 0 & 0 & 0 & 2G^b & 0 & 0 \\ 0 & 0 & 0 & 0 & 2G^b & 0 \\ 0 & 0 & 0 & 0 & 0 & 2G^b \end{bmatrix} \left\{ \begin{array}{c} d\varepsilon_x \\ d\varepsilon_y \\ d\varepsilon_z \\ d\varepsilon_{xy} \\ d\varepsilon_{yz} \\ d\varepsilon_{zx} \end{array} \right\}_b \tag{19}$$

In the bonded elements, the porosity was f^b_c and the volume occupied by the solid matrix was $1 - f^b_c$ According to the meso-mechanical method [14], the bulk modulus and shear modulus of the bonded elements can be obtained by:

$$K^b = K^s / \left[1 + f^b_c \frac{1}{1 - \alpha} \frac{K^S}{(1 - f^b_c)K^S} \right] \tag{20a}$$

$$G^b = G^s / \left[1 + f^b_c \frac{1}{1 - \beta} \frac{G^S}{(1 - f^b_c)G^S} \right] \tag{20b}$$

where K^S and G^S denote the bulk modulus and shear modulus of the coral-reef limestone matrix, respectively, In addition, α and β could be obtained from the inclusion theory [15], where $\alpha = \frac{3K^S}{3K^S + 4G^S}$; $\beta = \frac{6(K^S + 2G^S)}{5(3K^S + 4G^S)}$.

2.1.4. Stress–Strain Relationships for Frictional Elements

The frictional elements are elastic–plastic, and are assumed to be an elastic–plastic porous material composed of a solid soil skeleton with micro-scale pores. The elastic parameters and plastic stress–strain expressions at the meso-scale are obtained by the homogenization method. The strain increment of the frictional elements could be divided into elastic and plastic according to:

$$\{d\varepsilon\}_f = \{d\varepsilon^e\}_f + \left\{ d\varepsilon^f \right\}_f \tag{21}$$

For the elastic part of the frictional elements, the bulk modulus and shear modulus of the elastic parameters of the solid skeleton in the frictional elements are designated as K^M and G^M, respectively. The bulk modulus K^{fe} and shear modulus G^{fe} of the bonded elements could be obtained as follows [14,15]:

$$K^{fe} = K^M \frac{4(1 - \varphi)G^M}{3\varphi K^M + 4G^M} \tag{22a}$$

$$G^{fe} = G^M \frac{(1 - \varphi)(9K^M + 8G^M)}{K^M(9 + 6\varphi) + G^M(8 + 12\varphi)} \tag{22b}$$

The stress–strain relationship of the bonded elements follows:

$$\left\{ \begin{array}{c} d\sigma_x \\ d\sigma_y \\ d\sigma_z \\ d\tau_{xy} \\ d\tau_{yz} \\ d\tau_{zx} \end{array} \right\}_f = \begin{bmatrix} K^{fe} + \frac{4}{3}G^{fe} & K^{fe} - \frac{2}{3}G^{fe} & K^{fe} - \frac{2}{3}G^{fe} & 0 & 0 & 0 \\ K^{fe} - \frac{2}{3}G^{fe} & K^{fe} + \frac{4}{3}G^{fe} & K^{fe} - \frac{2}{3}G^{fe} & 0 & 0 & 0 \\ K^{fe} - \frac{2}{3}G^{fe} & K^{fe} - \frac{2}{3}G^{fe} & K^{fe} + \frac{4}{3}G^{fe} & 0 & 0 & 0 \\ 0 & 0 & 0 & 2G^{fe} & 0 & 0 \\ 0 & 0 & 0 & 0 & 2G^{fe} & 0 \\ 0 & 0 & 0 & 0 & 0 & 2G^{fe} \end{bmatrix} \left\{ \begin{array}{c} d\varepsilon_x^e \\ d\varepsilon_y^e \\ d\varepsilon_z^e \\ d\varepsilon_{xy}^e \\ d\varepsilon_{yz}^e \\ d\varepsilon_{zx}^e \end{array} \right\}_f \tag{23}$$

For the plastic part of the frictional elements, the D-P criterion is satisfied when yielding occurred, according to:

$$f^m(\sigma_{ij}^M) = -\sqrt{J_2^M} + \alpha'(\sigma_m^M + T) \tag{24}$$

where α' is the friction coefficient between the broken particles, T is the tensile strength (compression is positive) related to the cohesion and friction angle, and σ_{ij}^M is the stress of the solid phase, following $\sigma_m^M = \sigma_{ii}^M / 3$. In addition, the generalized shear stress will follow:

$$J_2^M = \frac{1}{2} S_{ij}^M S_{ij}^M,$$

where $s_{ij}^M = \sigma_{ij}^M - \sigma_M^M \delta_{ij}$, and δ_{ij} denotes the Kronecker symbol.

From the literature [16,17], the yield criterion can be expressed by the meso-scale D-P criterion (24) according to:

$$F\left(\sigma_m^f, \sigma_s^f, \varphi\right) = \frac{\left(\sigma_s^f\right)^2}{M} + A\left(\sigma_m^f - \sigma_m^c\right)^2 - \frac{(\alpha')^2 T^2 (1-\varphi)^2}{1 - \varphi - (\alpha')^2 K} \tag{25}$$

where $A = \frac{1}{K} - \frac{(\alpha')^2}{1-\varphi}$, $\sigma_m^c = (\alpha')^2 T/A$, $K = 4(1-\varphi)/3\varphi$, $M = (1-\varphi)/(1+\frac{2}{3}\varphi)$, f represents the frictional elements, and $\sigma_m^f = \frac{1}{3}\sigma_{kk}^f$, $\sigma_s^f = \sqrt{\frac{3}{2}s_{ij}^f s_{ij}^f}$, $s_{ij}^f = \sigma^f - \frac{1}{3}\sigma_{kk}^f \delta_{ij}$.

The plastic potential can be expressed by:

$$G\left(\sigma_m^f, \sigma_s^f, \varphi\right) = \frac{\left(\sigma_s^f\right)^2}{M\xi} + A\left(\sigma_m^f - \sigma_m^c\right)^2 - \frac{(\alpha')^2 T^2 (1-\varphi)^2}{1 - \varphi - \alpha^2 K} \tag{26}$$

where ξ is the model parameter. When using the associated flow rule, ξ will be 1.0.

According to the plastic theory, the plastic strain increment can be expressed by:

$$d\varepsilon_v^{fp} = d\lambda \frac{\partial G}{\partial \sigma_m^f} \tag{27}$$

$$d\varepsilon_s^{fp} = d\lambda \frac{\partial G}{\partial \sigma_s^f} \tag{28}$$

where $d\lambda$ is the plastic multiplier.

2.1.5. Structural Parameters

The structural parameters, including the breakage rate χ and local strain coefficient C_{ijkl}, and the optimal parameters are selected by trial and error.

The breakage rate reflects the degree of transformation from the breakage of the bonded elements to the frictional elements in the element. According to the initial breakage

state of the coral-reef limestone (influence of porosity) and the degree of breakage during the loading process, the following expression is adopted:

$$\chi = 1 - \exp\left[-c_1(\varepsilon_1)^{b_1}\right] \tag{29}$$

where a_1, b_1, c_1 are the model parameters and ε_1 is the axial strain.

The local strain coefficient C_{ijkl} establishes a relationship between the strain of the bonded elements and the strain of the unit. In this work, we adopted scalar C, as expressed by:

$$C = \exp\left[-c_0(\varepsilon_1)^{b_1}\right] \tag{30}$$

where c_0 is the model parameter, and the strain of the bonded elements during initial loading will be the strain of the frictional elements $C = 1.0$.

2.2. Determination of the Model Parameters under Uniaxial Compression Conditions

2.2.1. Determination of the Parameters of the Bonded Elements

Under triaxial stress state, the stress–strain relationship of the bonded elements could be simplified as:

$$\left\{ \begin{array}{c} d\sigma_1 \\ d\sigma_3 \end{array} \right\}_b = \left[\begin{array}{cc} K^b + \frac{4}{3}G^b & 2(K^b - \frac{2}{3}G^b) \\ K^b - \frac{2}{3}G^b & 2(K^b + \frac{1}{3}G^b) \end{array} \right] \left\{ \begin{array}{c} d\varepsilon_1 \\ d\varepsilon_3 \end{array} \right\}_b \tag{31}$$

2.2.2. Parameter Determination of the Frictional Elements

Under triaxial stress state, the elastic stress–strain relationship of the frictional elements could be simplified as:

$$\left\{ \begin{array}{c} d\sigma_1 \\ d\sigma_3 \end{array} \right\}_f = \left[\begin{array}{cc} K^{fe} + \frac{4}{3}G^{fe} & 2(K^{fe} - \frac{2}{3}G^{fe}) \\ K^{fe} - \frac{2}{3}G^{fe} & 2(K^{fe} + \frac{1}{3}G^{fe}) \end{array} \right] \left\{ \begin{array}{c} d\varepsilon_1^e \\ d\varepsilon_3^e \end{array} \right\}_f \tag{32}$$

Equation (32) could also be transformed into $d\sigma_m^f = K^{fe}d\varepsilon_v^{fe}$, $d\sigma_s^f = 3G^{fe}d\varepsilon_s^{fe}$. By substituting these two equations, the incremental expression of elasticity could be obtained:

$$d\sigma_m^f = K^{fe}\left(d\varepsilon_v^f - d\lambda \frac{\partial G}{\partial \sigma_m^f}\right) \tag{33a}$$

$$d\sigma_s^f = 3G^{fe}\left(d\varepsilon_s^f - d\lambda \frac{\partial G}{\partial \sigma_s^f}\right) \tag{33b}$$

Considering the consistency condition, $df = \frac{\partial F}{\partial \sigma_m^f}d\sigma_m^f + \frac{\partial F}{\partial \sigma_s^f}d\sigma_s^f = 0$, by substituting Equation (33a,b) into the equation, we obtained $d\lambda$ by:

$$d\lambda = \frac{1}{H}\left(K^{fe}\frac{\partial F}{\partial \sigma_m^f}d\varepsilon_v^f + 3G^{fe}\frac{\partial F}{\partial \sigma_s^f}d\varepsilon_s^f\right) \tag{34}$$

where $H = K^{fe}\frac{\partial F}{\partial \sigma_m^f}\frac{\partial G}{\partial \sigma_m^f} + 3G^{fe}\frac{\partial F}{\partial \sigma_s^f}\frac{\partial G}{\partial \sigma_s^f}$.

From this, the incremental stress–strain relationship of the frictional elements could be established:

$$d\sigma_m^f = C_{mm}^f d\varepsilon_v^f + C_{ms}^f d\varepsilon_s^f \tag{35a}$$

$$d\sigma_s^f = C_{sm}^f d\varepsilon_v^f + C_{ss}^f d\varepsilon_s^f \tag{35b}$$

where:

$$C_{mm}^f = K^{fe}(1 - K^{fe}\frac{1}{H}\frac{\partial F}{\partial \sigma_m^f}\frac{\partial G}{\partial \sigma_m^f}), C_{ms}^f = -3G^{fe}K^{fe}\frac{1}{H}\frac{\partial F}{\partial \sigma_s^f}\frac{\partial G}{\partial \sigma_m^f}, C_{sm}^f = -3G^{fe}K^{fe}\frac{1}{H}\frac{\partial F}{\partial \sigma_m^f}\frac{\partial G}{\partial \sigma_s^f},$$

$$C_{ss}^F = 3G^{fe}(1 - 3G^{fe}\frac{1}{H}\frac{\partial F}{\partial \sigma_s^f}\frac{\partial G}{\partial \sigma_s^f}), \frac{\partial G}{\partial \sigma_m^f} = 2A(\sigma_m^f - \sigma_m^c); \frac{\partial G}{\partial \sigma_s^f} = 2\frac{\sigma_s^f}{M\xi}, \frac{\partial F}{\partial \sigma_m^f} = 2A(\sigma_m^f - \sigma_m^c), \frac{\partial F}{\partial \sigma_s^f} = 2\frac{\sigma_s^f}{M}.$$

2.2.3. Determination of Structural Parameters

Under triaxial stress conditions, the expressions of the breakage rate and local strain coefficient follows:

$$\chi = 1 - \exp\left[-c_1(\varepsilon_1)^{b1}\right] \tag{36}$$

$$C = \exp\left[-c_0(\varepsilon_1)^{b1}\right] \tag{37}$$

3. Comparisons of the Tested and Model Predicted Results

To clarify the constitutive model of the coral-reef limestone, relevant parameters were obtained by conducting relevant experiments. Among these, the porosity f_c^b was determined by the porosity test, while the matrix parameters of the bulk modulus and shear modulus were solved according to the bonded strength and uniaxial testing. Thus, a constitutive model of the coral-reef limestone in the sample area was formed.

3.1. Uniaxial Compressive Strength

The coral-reef limestone samples were subjected to uniaxial compression testing, where each sample is 50 mm in diameter and 100 mm in height, and the displacement control method was used for loading at a loading rate of 0.002 mm/s. Figure 3 shows the photos of the samples.

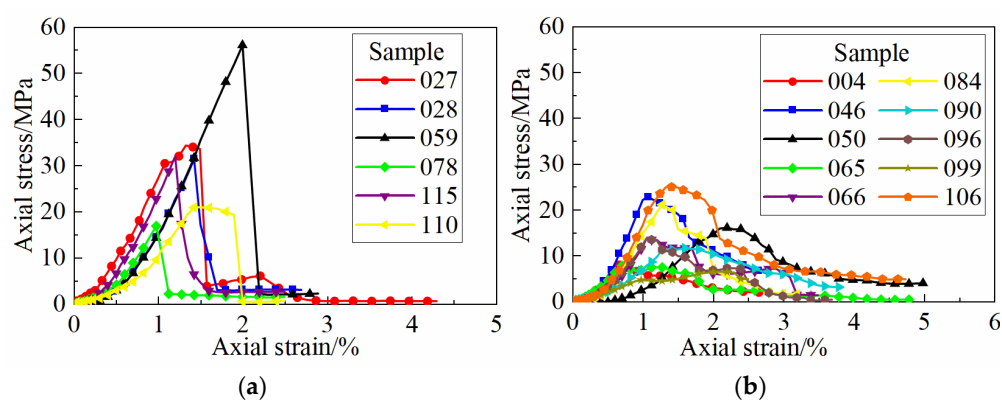**Figure 3.** Saturated uniaxial compression specimen.

Uniaxial compression testing was conducted on 16 samples to obtain the stress–strain curves of the coral-reef limestone. The measured peak strength of the coral-reef limestone ranges from 7–56 MPa, and the average strength is 21 MPa. The strain corresponding to the peak strength is between 0.70% and 2.19%, and the average peak strain is 1.34%. The elastic modulus ranges from 3–28 GPa, and the average elastic modulus is 16 GPa. The test results

are shown in Table 1. The strength and elastic modulus of the coral-reef limestone are low and widely distributed, with strong discreteness. This is related to the unique diagenesis and epigenetic evolution of the coral-reef limestone, while its strength is mainly determined by the strength of its constituent minerals and the degree of mineral cementation.

Table 1. Uniaxial compression test results.

Sample	Uniaxial Compressive Strength (MPa)	Peak Strain (%)	Elastic Modulus (GPa)	Failure Mode
027	34	1.32	26	Brittle failure
028	32	1.42	22	Brittle failure
059	56	1.99	28	Brittle failure
078	17	0.97	18	Brittle failure
110	21	1.49	14	Brittle failure
115	32	1.20	27	Brittle failure
004	8	0.66	12	Ductile failure
046	23	1.07	21	Ductile failure
050	16	2.19	7	Ductile failure
065	8	0.70	11	Ductile failure
066	14	1.05	13	Ductile failure
084	21	1.27	17	Ductile failure
090	12	1.59	7	Ductile failure
096	14	1.05	13	Ductile failure
099	7	2.09	3	Ductile failure
106	25	1.32	19	Ductile failure
Mean	21	1.34	16	

The principal stress–axial curves of all samples are presented in Figure 4. The compressive failure modes include brittle failure (samples 027, 028, 059, 078, 110, and 115) and ductile failure (samples 004, 046, 050, 065, 066, 084, 090, 096, 099, and 106). Before reaching ultimate strength, the axial stress–strain curves of the two failure modes show a constant increasing trend, and the stress drops sharply after reaching peak strength in brittle failure. Thus, the bearing capacity is quickly lost. After reaching peak strength, the samples with ductile failure do not completely fail. The bearing capacity gradually decreases and the strain further increases. The post-peak stress drop rate is small, which is quite different from the failure mode of brittle rock, indicating the existence of large residual strength after the failure of the coral-reef limestone.
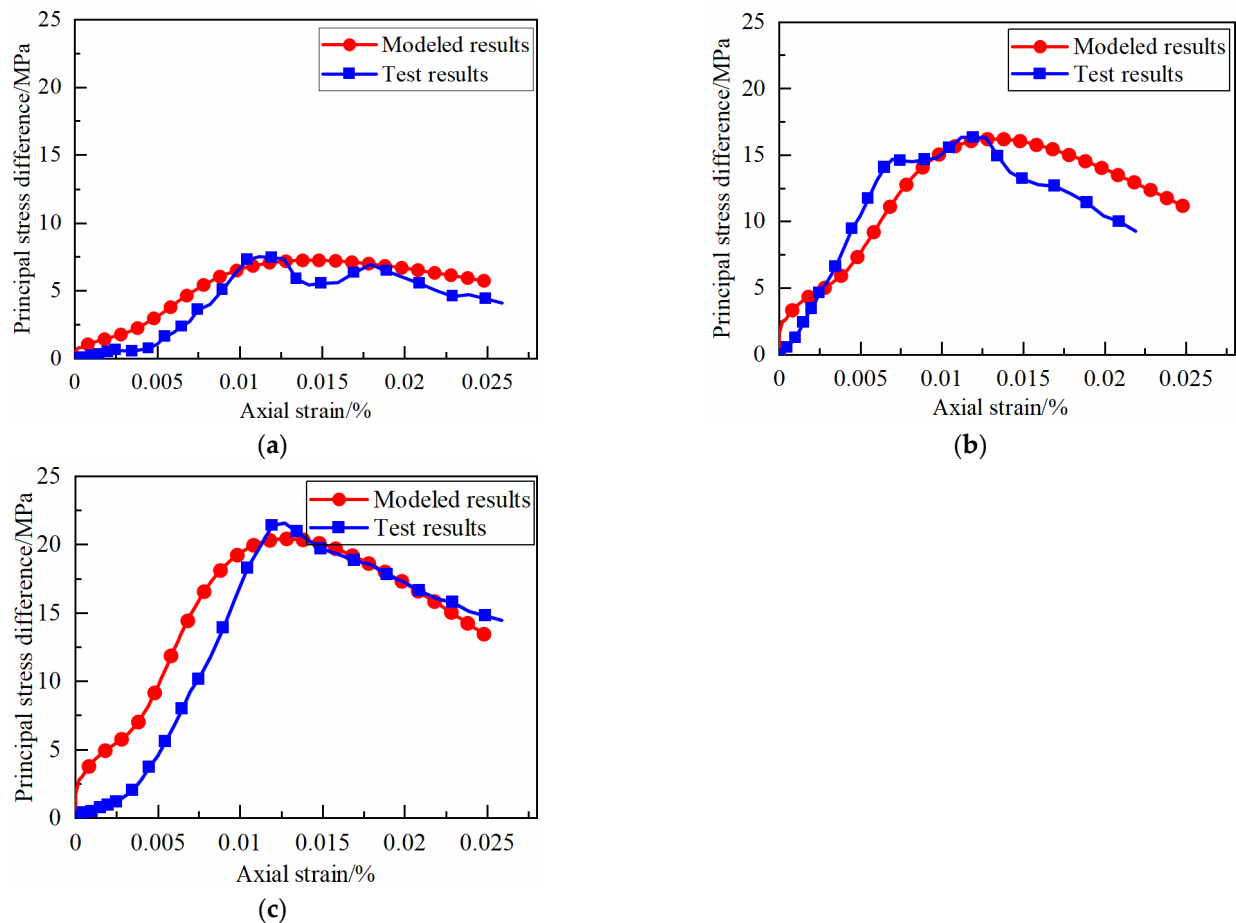

Figure 4. Stress–strain curves of the coral-reef limestone under uniaxial compression testing: (**a**) brittle failure and (**b**) ductile failure.

3.2. Verification of Constitutive Model

To prove the reliability of the coral-reef limestone constitutive model, the test results were compared with the modeled results (Figure 5) according to the stress–strain curve of

coral-reef limestone under uniaxial compression. The calculated parameters were as follows. The porosity values of samples 1, 2, and 3 were 0.17, 0.20, and 0.18, respectively, and the values of K^S, G^S, K^M, and G^M are shown in Table 2, where K^s and G^S are determined according to the test results of the sample in the initial stage of loading, and K^M and G^M are determined by the test results of the sample in the residual stage of loading. In addition, $\alpha' = 0.48$, $\xi = 2.5$, and $T = 0.2$ MPa, where the porosity of the frictional elements is 1.1 times that of the bonded elements, and $b_1 = 0.452$, $c_1 = 23.5$, and $c_0 = 0.2$. Figure 5 shows that the calculated results are basically consistent with the test results, which reflects the strain-softening phenomenon.

Figure 5. Verification of uniaxial compressive stress–strain curves of coral-reef limestone: (**a**) sample 1, (**b**) sample 2, and (**c**) sample 3.
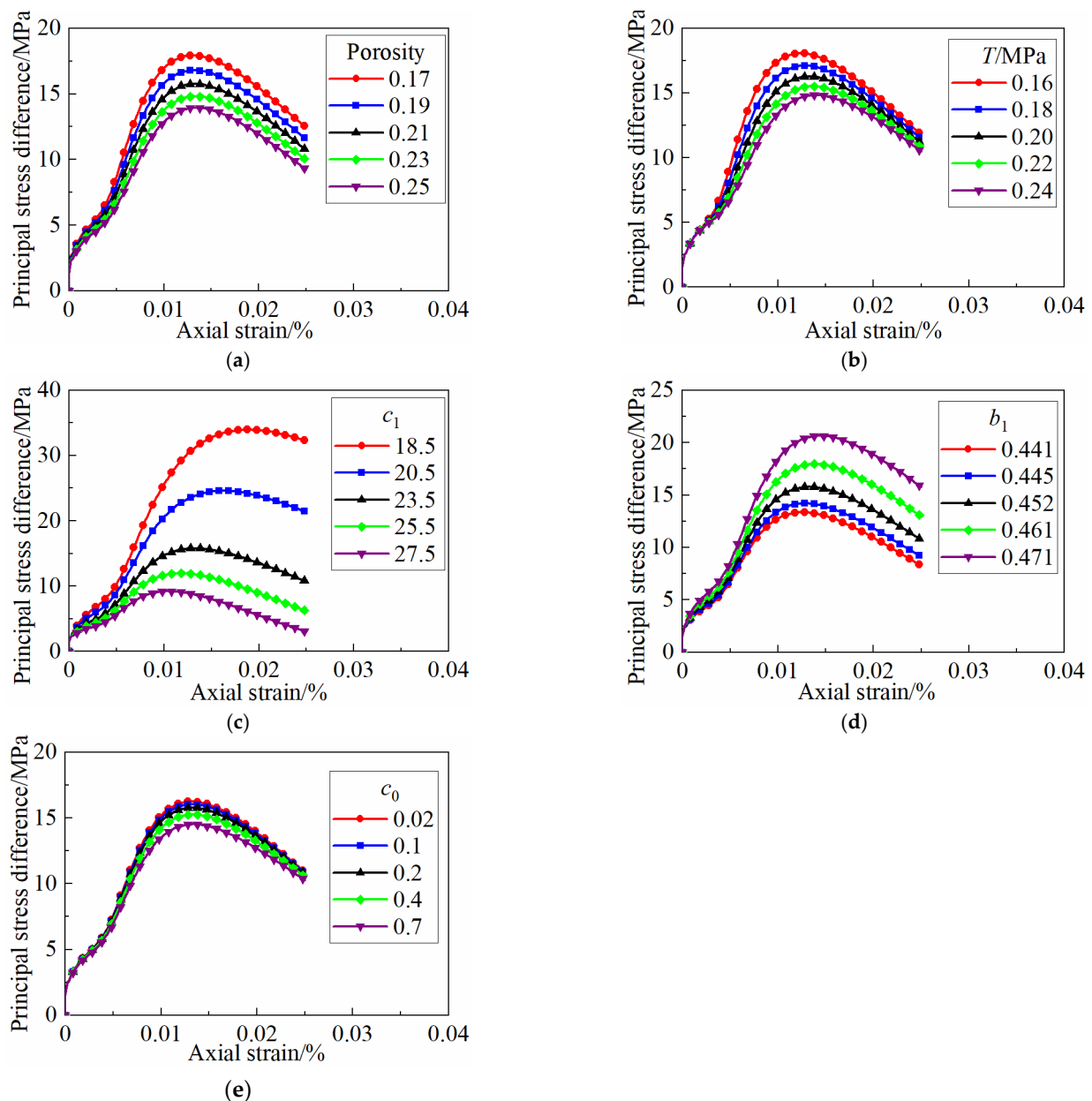
Table 2. Parameter values of K^S, G^S, K^M, and G^M.

Parameters	Sample 1 (MPa)	Sample 2 (MPa)	Sample 3 (MPa)
K^S	7430.4	15,170.4	18,808.2
G^S	1218	4350	4640
K^M	39.84	83.01	86.33
G^M	31.51	38.15	39.81

3.3. Analysis of Varying Parameters

Figure 6 presents the parameter sensitivity analysis results, where the influence of porosity, T, c_1, b_1, and c_0 on the principal stress difference are analyzed. The changes in the porosity, T, $c_{1\ 1}$, b_1, and c_0 all affect the principal stress difference. With an increasing sample porosity, the peak principal stress difference gradually decreases; however, the

overall change trend remains the same, as shown in Figure 6a. As T increases, the peak principal stress difference decreases (see Figure 6b). Thus, the influence of c_0 on the principal stress difference is obvious. The peak principal stress difference corresponding to the minimum c_1 value is approximately five times that of the maximum c_1 value. With an increasing c_1, the peak principal stress difference gradually decreases, and the reduction amplitude increases with increasing deformation (Figure 6c). The influence of b_1 on the principal stress difference is similar to that of c_1; however, the reduction amplitude is less than that of c_1, as shown in Figure 6d. Therefore, the influence of c_0 on the principal stress difference is insignificant. With increasing c_0, the peak principal stress difference gradually decreases, and the decrease in amplitude is small, as illustrated in Figure 6e.

Figure 6. Effects of parameter changes on the uniaxial compressive stress–strain curves of coral-reef limestone: (**a**) porosity, (**b**) *T*, (**c**) c_1, (**d**) b_1 and (**e**) c_0.

3.4. Analysis of Varying Parameters

In the paper, a new binary-medium-based constitutive model for coral reef lime-stone is proposed, which can simulate the strain softening easily under unconfined conditions.

When formulating the constitutive model, the nonuniform distribution of cementations and big pores are considered, within which, the stain and strain of the bonded element and frictional elements are different, and thus, in the process of loading, the bonded elements break up gradually and transform into frictional elements. In the model, the breakage of cementations can be simulated by the mechanical features of the bonded elements and the breakage ratio, so the strain softening can be duplicated easily under unconfined conditions. Furthermore, the bonded element is poroelastic and consists of solid matrix and pores, and the frictional element is an elastic–plastic porous material composed of a solid skeleton and pores. Using a homogenization approach, the mechanical parameters in micro and macro scales are linked. That is to say, the parameters in the constitutive model has a relatively clear physical meaning compared with the traditional ones.

In the current study, only the test results under unconfined stress conditions were compared, which can be extended to conditions with confining stress conditions in the near future. For the determination of model parameters, tests with a smaller size of the sample can be carried out with the development of a measurement technique, which can obtain the fundamental parameters, such as the frictional coefficient and tensile strength elastic modulus at a very small size.

The following is Table 3, which demonstrates the advantages and disadvantages of methods developed/applied on UCS-based modeling and experiments.

Table 3. Advantages and disadvantages of methods developed/applied on UCS-based modeling and experiments.

Advantage	Disadvantage
Tests easily performed; Relatively simple stress state; Laws easily found.	Complex stress states can be reflected.

4. Conclusions

The pile foundation has strong competitiveness in the construction of sea crossing bridges and large offshore platforms that require a large bearing capacity, stability, and reliability of the foundation. Under the geological condition of a coral reef, the cast-in pile is preferred because the driven pile has a low lateral resistance and low bearing efficiency. The vertical bearing capacity of the filling section is closely related to the rock strength of reef limestone, so the constitutive model suitable for reef limestone is the key to putting forward the design method of a filling pile in reef limestone strata. Based on the uniaxial compression test results of coral-reef limestone, a binary-medium-based constitutive model of coral-reef limestone was established, and the test results were verified. The key conclusions are as follows.

(1) According to the concept of the binary medium model, the coral-reef limestone is regarded as a binary medium material composed of bonded and frictional elements. A constitutive model of the coral-reef limestone was constructed based on the homogenization theory, where the established constitutive model considers the cementation and pore distribution of coral-reef limestone.

(2) The uniaxial compression tests on coral-reef limestone demonstrates that coral-reef limestone contains strain-hardening characteristics. The parameter determination method for the binary-medium-based constitutive model was adopted based on uniaxial compression testing. A comparison with the test results confirmed that the proposed method is reasonable.

(3) The parameter sensitivity analysis of the model shows that changes in the main parameters of the model reflects the strain softening degree of coral-reef limestone, thus providing a basis for the basic design of coral-reef limestone.

Author Contributions: Visualization, Y.C.; Writing—original draft, Y.Z., H.L., P.C. and E.L. All authors have read and agreed to the published version of the manuscript.

Conflicts of Interest: The authors declare no conflict of interest.

References

1. Cargill, J.S.; Shakoor, A. Evaluation of empirical-methods for measuring the uniaxial compressive strength of rock. *Int. J. Rock Mech. Min. Sci.* **1990**, *27*, 495–503. [CrossRef]
2. Zhang, C.; Liang, W.; Li, Z.; Xu, S.; Zhao, Y. Observations of acoustic emission of three salt rocks under uniaxial compression. *Int. J. Rock Mech. Min. Sci.* **2015**, *77*, 19–26. [CrossRef]
3. Singh, A.; Kumar, C.; Kannan, L.G.; Rao, K.S.; Ayothiraman, R. Estimation of creep parameters of rock salt from uniaxial compression tests. *Int. J. Rock Mech. Min. Sci.* **2018**, *107*, 243–248. [CrossRef]
4. Azarafza, M.; Ghazifard, A.; Akgun, H.; Asghari-Kaljahi, E. Geotechnical characteristics and empirical geo-engineering relations of the South Pars Zone marl, Iran. *Geomech. Eng.* **2019**, *19*, 393–405.
5. Azarafza, M.; Ghazifard, A.; Asasi, F.; Rahnamarad, J. An empirical classification method for South Pars marls by Schmidt hammer rebound index. *MethodsX* **2021**, *8*, 101366. [CrossRef] [PubMed]
6. Yu, D.; Liu, E.; Sun, P.; Xiang, B.; Zheng, Q. Mechanical properties and binary-medium constitutive model for semi-through jointed mud-stone samples. *Int. J. Rock Mech. Min. Sci.* **2020**, *132*, 104376. [CrossRef]
7. Yesiloglu-Gultekin, N.; Gokceoglu, C. A Comparison Among Some Non-linear Prediction Tools on Indirect Determination of Uniaxial Compressive Strength and Modulus of Elasticity of Basalt. *J. Nondestruct. Eval.* **2022**, *41*, 1–24.
8. Yu, M.; Wu, M.; Yang, X.; Lou, R.; Wang, F.; Li, H.; Wang, L. Effect of temperature on the evolution and distribution for particle size of loose broken coal during the uniaxial confined compression process. *Fuel* **2022**, *134*, 123592. [CrossRef]
9. Wan, Z.; Dai, G.; Gong, W. Full-scale load testing of two large-diameter drilled shafts in coral-reef limestone formations. *Bull. Eng. Geol. Environ.* **2018**, *77*, 1127–1143. [CrossRef]
10. Tang, Q.; Zhang, J.; Feng, Y.; Li, J.; Yao, Y.; Sun, J.; Zhan, W. Numerical Simulation for Shallow Strata Stability of Coral Reef in the Southwest of Yongshu Reef (South China Sea). *J. Ocean Univ. China* **2018**, *17*, 763–772. [CrossRef]
11. Li, D.J.; Shi, C.; Ruan, H.N.; Li, B.Y.; Li, W.Y.; Yao, X.C. Study on shear behavior of coral reef limestone–concrete interface. *Mar. Georesources Geotechnol.* **2021**, *40*, 438–447. [CrossRef]
12. Shen, Z.J. Progress in binary medium modeling of geological materials. In *Modern Trends in Geomechancis*; Springer: Berlin/Heidelberg, Germany, 2006; pp. 77–99.
13. Liu, E.L.; Yu, H.S.; Zhou, C.; Nie, Q.; Luo, K.T. A binary-medium constitutive model for artificially structured soils based on the disturbed state concept (dsc) and homogenization theory. *Int. J. Geomech.* **2017**, *17*, 04016154. [CrossRef]
14. Mura, T. Micromechanics of defects in solids. *J. Acoust. Soc. Am.* **1983**, *73*, 2237. [CrossRef]
15. Eshelby, J.D. The determination of the elastic field of an ellipsoidal inclusion and related problems. *Proc. R. Soc. London. Ser. A. Math. Phys. Sci.* **1957**, *241*, 376–396.
16. Dormieux, L.; Kondo, D.; Ulm, F.J. Microporomechanics (Dormieux/Microporomechanics). In *Microporoplasticity*; John Wiley & Sons: Hoboken, NJ, USA, 2006. [CrossRef]
17. Maghous, S.; Dormieux, L.; Barthèlémy, J.F. Micromechanical approach to the strength properties of frictional geomaterials. *Eur. J. Mech. A-Solid* **2009**, *28*, 179–188. [CrossRef]